Desalination and Water Treatment
www.deswater.com

doi: 10.1080/19443994.2016.1155179

57 (2016) 25747–25756
November

Taylor & Francis
Taylor & Francis Group

Magnesium recovery from brines using exopolymeric substances of sulfate-reducing bacteria

Abdul-Matiin Wan[a], Bilal Mansoor[b], Farrukh Ahmad[a,*]

[a]*Bio-Energy and Environmental Laboratory (BEEL), Institute Center for Water and Environment (iWATER), Masdar Institute of Science and Technology, P.O. Box 54224, Abu Dhabi, UAE, email: amwan@b2el.com (A.-M. Wan), Tel. +971 2 810 9114; Fax: +971 2 810 9901; email: fahmad@masdar.ac.ae (F. Ahmad)*
[b]*Mechanical Engineering Program, Texas A&M University at Qatar, P.O. Box 23874, Doha, Qatar, email: bilal.mansoor@qatar.tamu.edu*

Received 22 December 2015; Accepted 13 February 2016

ABSTRACT

Magnesium recovery from brines was studied *ex situ* under sulfate-reducing conditions and in the presence of active cells and exopolymeric substances (EPS) using an innovative experimental approach. EPS was extracted and a mixed sulfate-reducing inoculum was enriched from dolomitizing coastal microbial mats. The inoculum tested positive for the presence of the *Desulfovibrio brasiliensis*, the organism associated with biogenic dolomitization, using denaturing gradient gel electrophoresis. Cultures were incubated within dialysis tubes, together with TEM grids that provided an imaging-ready substratum for biofilm growth and mineral precipitation. The anaerobic incubations lasted 16 d under a continually increasing bulk solution magnesium ion concentration. The following reactor configurations were incubated: (A) bacteria-only, (B) bacteria + pre-extracted EPS, (C) pre-extracted EPS-only, and (D) control. The TEM grids were recovered for analysis using spot, line transect, and areal SEM–energy-dispersive X-ray analysis for elemental comparison of deposits. Pre-extracted EPS-bearing cultures, both with and without bacterial inoculum, induced surface-associated magnesium recovery in 16 d. Overall, magnesium recovery in the EPS-only system was 2.2*x* (line transect) to 1.5*x* (areal) greater than the bacteria + EPS system, while the bacteria-only (*de novo* EPS only) and control (no EPS) reactors displayed no surface-associated magnesium recovery. Analysis of microstructures within the bacteria + pre-extracted EPS system revealed variations in the Mg:Ca ratios, ranging from 19.9 to 61.9% (spot analysis) over different deposit morphologies, suggesting a dynamic biologically mediated mineralization process for magnesium recovery from brines requiring further investigation.

Keywords: Magnesium; Brine; Biomineralization; Exopolymeric substances (EPS); Sulfate-reducing bacteria (SRB)

1. Introduction

Magnesium is a light metal that is extensively used in alloys owing to its high strength to weight ratio [1] leading to many applications in transportation, electronics, and biomedical devices. Currently, China meets 80% of the world demand for magnesium metal, producing it via the Pidgeon process, a thermal catalytic reduction process that uses silicon as the

*Corresponding author.

catalyst and magnesia (i.e. magnesium oxide [MgO]) as the starting materials [2]. Magnesia, in turn, is produced from the calcination of magnesium-based carbonates such as magnesite, dolomite, and other calcium–magnesium carbonates [3], deposits of which are ancient and limited around the world. While electrolytic processes for magnesium recovery from saline water sources like seawater do exist (e.g. the Dow Process [3]) and while their application to brines has been proposed [4], these processes remain widely unpopular because of their high capital and energy costs [2]. On the other hand, more traditional salt recovery processes like evaporation of desalination retentate [5] have shown limited success in selective mineral precipitation and instead produce mixtures of salts. More recently, new processes such as eutectic point freezing [6] and membrane distillation [7] have been tested at the small scale, but these might prove difficult to implement on a larger scale because of their high costs unless one or more commercially viable products can be recovered.

Although dissolved magnesium is readily available in seawater (at approx. 1.60 g/L in the Arabian Gulf [4]), thermal desalination brines (at approx. 2.75 g/L [4]), and coastal groundwater (at approx. 3.75–7.80 g/L in Abu Dhabi [8–10]), its precipitation as a mineral under ambient or near-ambient temperatures and pressures is generally not observed even though a number of its carbonates (e.g. magnesite and dolomite) are thermodynamically favored to precipitate. However, the coastal sabkhas (salt flats) of western Abu Dhabi (UAE), alongside a handful of other locations with hypersaline water, like Lagoa Vermelha and Brejo do Espinho (Brazil), the Coorong (Australia), Madrid Basin (Spain), and Qinghai Lake (China), have been reported to host ongoing dolomite, magnesite, and Mg–calcite formation in close association with biological activity [11–15]. The usually hypersaline and sulfate-rich environments of these sites accommodate sulfate-reducing bacteria (SRB) communities hypothesized to overcome the kinetic barrier through cation–sulfate pair dissociation and subsequent sulfate reduction into sulfide [16,17]. These sites have all demonstrated the presence of an organism capable of biogenic dolomitization, *Desulfovibrio brasiliensis*. Yet, little is known of the mechanism of dolomitization with this organism.

Beyond the interplay of dissolved chemical ions, the structural components of the resident biofilms also merit further investigation for their role in biomineralization. This is particularly important in explaining observations of biomineralization in both microbially active and inactive communities [11]. Hence, there is growing interest in exopolymeric substances (EPS), the substance comprising much of the biofilm matrix. The complex mix of polysaccharides, proteins, nucleic acids, and lipids [18] that make up EPS may provide favorable conditions to drive biomineralization, in addition to their role in supporting community surface adhesion, structural integrity, and chemical buffering [19]. Previous work speculates the involvement of EPS components such as negatively charged polyanions acting as cation-complexing "microenvironments" conducive to Ca–Mg carbonate biomineralization [20–23].

This paper presents a proof-of-concept study of magnesium recovery under *ex situ* sulfate-reducing conditions using components of biofilms (e.g. pre-extracted EPS, cells, or both) extracted from a microbial mat from a coastal sabkha site in Abu Dhabi. Extracted EPS was applied to a hypersaline medium (brine) with and without bacterial inoculation to investigate the influence of pre-extracted EPS on magnesium recovery. Moreover, the experiment employed the novel approach of compartmentalized culture growth within dialysis tubes under anaerobic conditions and co-incubated inert solid substrata to enable imaging and analysis of surface-attached growth and precipitation. This study represents a first step toward a potential process involving low-energy bio-mediated beneficial mineral recovery from seawater brine waste streams.

2. Materials and methods

2.1. Inoculum and EPS extract preparation

Mixed cultures were enriched out of upper intertidal sediment samples from a coastal sabkha site previously investigated for dolomite deposition [11]. Growth conditions were selective for sulfate reduction, prepared using the Postgate medium [11,24] containing: KH_2PO_4 (3.67 mM), NH_4Cl (18.69 mM), $CaCl_2$ (0.68 mM), $MgSO_4{\cdot}7H_2O$ (12.17 mM), potassium lactate (42.9 mM), $FeSO_4{\cdot}7H_2O$ (3.29 mM), and yeast extract (1 g/L). Medium pH was adjusted and maintained at 7.5 with NaOH. Enrichment cultures were then processed to produce inoculum and EPS designated for downstream *ex situ* mineralization experiments. EPS extraction was performed on four-day old cultures based on the procedure of Hung et al. [25], targeting both the dissolved EPS and particulate EPS fractions (Supplementary Figures S1(a) and (b), respectively).

2.2. Ex situ biomineralization experimental setup

A series of customized 500-mL pre-autoclaved anaerobic reactors were set up to accommodate mixed-culture growth in a dynamic hypersaline

medium (modified from Postgate [24]) designed to simulate the increasing pore water hardness (Mg^{2+} and Ca^{2+} content) of Abu Dhabi's coastal sabkhas post-tidal flooding and evaporitic conditions [26]. The increasing divalent cation concentration gradient ensured the bulk solution saturation state for dolomite, magnesite, aragonite, and calcite (Table 1) over the limited experimental duration of 16 d. Shallow groundwater from a local coastal site, which happens to be hypersaline [10], was previously characterized to contain: Mg^{2+} (256.5 mM), Ca^{2+} (65.75 mM), Na^{+} (3,415.2 mM), SO_4^{2-} (34.23 mM) and Cl^{-} (4,027.2 mM).

The initial composition of the growth medium was designed to contain: KH_2PO_4 (3.67 mM), NH_4Cl (18.69 mM), $CaCl_2$ (5.1 mM), $MgSO_4{\cdot}7H_2O$ (31.64 mM), potassium lactate (53.45 mM), $FeSO_4{\cdot}7H_2O$ (0.03 mM), ferric citrate (1.02 mM), NaCl (444.88 mM), $NaHCO_3$ (29.76 mM), yeast extract (1 g/L), vitamin solution (1% v/v), and sodium resazurin (0.004 mM). Final pH was set at 8.0 for the experiment. The gradual increase in water hardness was accomplished by periodic and incremental loading of the system with Mg^{2+} and Ca^{2+} (final concentrations 62.89 mM and 24.96 mM, respectively). Inoculation of the reactors was done in 1-mL Float-A-Lyzer® G2 dialysis units (3 kDa; Spectrum Labs, CA, USA) to maintain compartmentalized growth in the reactors. The dialysis membrane separated bacterial cells and mineral precipitates from the greater environment in the reactor, while allowing transfer of metabolites and nutrients.

The reactors hosted the following combinations of bacteria and pre-extracted EPS: A (bacteria-only), B (bacteria + pre-extracted EPS), and C (pre-extracted EPS-only), with a control set containing only sterile medium (Fig. 1). Three alphanumeric transmission electron microscope (TEM) grids (3.05 mm, gold; Electron Microscopy Sciences, PA, USA) were also incubated in each dialysis unit as substratum conducive to imaging of surface-attached growth and mineral deposition. All reactors were incubated in the dark at 35°C (ambient temperature to simulate field conditions) inside an anaerobic chamber (A35, Don Whitley Scientific, UK; $H_2/CO_2/N_2$ at 5%/15%/80% by volume) for 16 days. The bulk volume within each reactor was sampled (20-mL sample/reactor) every 48 h from the commencement of the experiment (Day 0). Twenty milliliters of sterile replacement medium were administered to each reactor following every periodic sampling of bulk volume. The composition of the replacement medium was identical to the growth medium except for the incremental concentrations of Mg^{2+} and Ca^{2+} (supplemented in the form of $MgCl_2$ and $CaCl_2$, respectively) (Supplementary Table S1). Changes in the bulk media chemistry were modeled with Geochemist's Workbench® software (Aqueous Solutions, IL, USA). Saturation index (SI) values of various carbonate minerals were determined at each time point using the Harvie–Møller–Weare (HWM) virial method [27], based on the expected periodic molar concentrations of ionic species. The HWM method is based on Pitzer's virial expansion model, and utilizes a partially experimentally validated ion interaction parameters database for Na–K–Mg–Ca–H–Cl–SO_4–OH–HCO_3–CO_3–CO_2–H_2O [28]. Unlike PHR EEQC and MINTEQ, this geochemical modeling approach allows for a more accurate prediction of activity coefficients and saturation indices in saline and hypersaline water, including brines, with a few limitations [29]. The SI calculations described the system as already supersaturated with respect to dolomite, magnesite, calcite, and aragonite over the course of the experiment (Table 1), as indicated by their positive values. TEM grids were recovered from the dialysis tubes at the completion of the 16-day experiment.

Table 1
SI values of minerals in bulk solution

Mineral	Day 0	Day 8	Day 16
Dolomite[a]	4.52	4.91	5.39
Dolomite[b]	2.98	3.37	3.85
Magnesite	1.58	1.71	1.83
Calcite	1.31	1.57	1.93
Aragonite	1.14	1.41	1.77
Gypsum	−1.17	−0.93	−0.60
Anhydrite	−1.34	−1.09	−0.76
Hydromagnesite	−1.68	−1.03	−0.40
Halite	−2.60	−2.58	−2.53

Notes: $MgCl_2$ and $CaCl_2$ were incrementally added every other day over a 16-day period. The activity coefficients for the saturation indices were determined using the Harvie–Moller–Weare virial method applicable to high ionic strength solutions. Positive SI values indicate supersaturated conditions in the aqueous solution with respect to the mineral. Dolomite notations "a" and "b" refer to ordered and disordered dolomite, respectively.

2.3. Analytical methods

2.3.1. EPS characterization

Alcian blue staining was subsequently performed on resuspended EPS extract to verify EPS presence, based on approaches taken by Tamaru et al. [30] and Ercole et al. [21]. A smear was made on a glass slide and heat-fixed by briefly passing the slide over a flame. The slide was then placed in 3% acetic acid (v/v) for 30 min, then in Alcian blue reagent (pH 2.5) containing 0.33% Alcian Blue 8GX (w/v) in 30% acetic

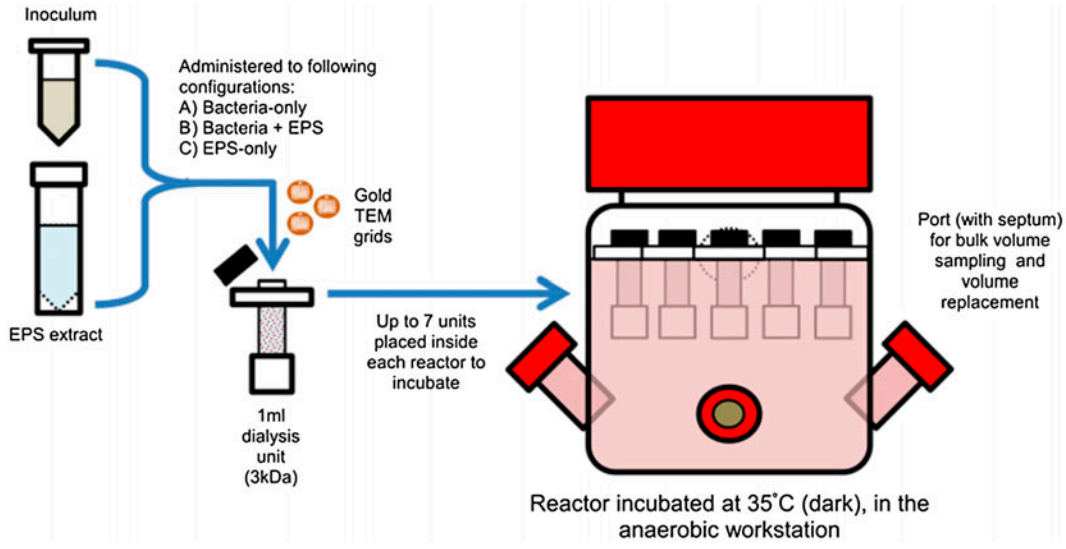

Fig. 1. Experimental setup comprising dialysis cultures of sabkha sulfate-reducing bacteria and EPS in 400 mL of bulk medium. Cultures were incubated with TEM grids for 16 d under anaerobic conditions and at the following configurations: (A) bacteria-only (inoculum: sterile medium: EPS extract at 0.05 mL: 0.95 mL: 0 mL), (B) bacteria + EPS (0.05 mL: 0.25 mL: 0.70 mL), (C) EPS-only (0 mL: 0 mL: 1 mL), and (D) control (0 mL: 1 mL: 0 mL).

acid and 70% ethanol (v/v) for another 30 min. The staining procedure was repeated using Alcian blue reagent at pH 0.5 on a second smear prepared from the suspension. Prepared slides were observed with an optical microscope up to 100× magnification. The appearance of the stained EPS extracts was also compared with that of biofilm-associated EPS, by staining a smear from one of the cultures. The carbohydrate/polysaccharide content of the EPS extract was also characterized using the Phenol–Sulfuric Acid assay [31], with glucose as a standard.

2.3.2. Medium chemistry

The bulk volume samples (each 20 mL) were filtered with a 0.22-μm syringe filter in preparation for chemical analysis. Anion and cation content was measured by ion chromatography (IC)(ICS-3,000, Dionex, CA, USA) following the methods of Farhat et al. [32]. Analysis was done only at the 8-day and 16-day mark.

2.3.3. Microbial ecology

The inoculum and culture solution from dialysis units were processed for DNA extraction using the UltraClean® Soil DNA Isolation Kit (MO BIO Laboratories, CA, USA) following the vendor's recommended protocol. Extracted DNA was then processed for denaturing gel gradient electrophoresis (DGGE) for the analysis of communities across reactors, and against a pure culture of dolomite-mediating SRB, *D. brasiliensis* (Deutsche Sammlung von Mikroorganismen und Zellkulturen [DSMZ], Germany). The DGGE protocol used was described in a prior publication [33] with a modification of the denaturant range from 20 to 60%.

2.3.4. Mineralogy

X-ray diffraction (XRD) analysis was performed to determine the identity of minerals deposited. The analysis was performed on mineral associated from the dialysis tube broth as there were too few minerals by mass associated with the TEM girds to be separated from the metal grid and prepared for XRD analysis. Sample preparation involved recovery of the culture solution from the dialysis units, centrifugation at 18,000× *g*, bleaching the pellet with NaOCl (5%), further centrifugation at 18,000× *g*, and final rinse with deionized water. The remaining product was air dried, powdered, and analyzed using an AXS D8 Advance, equipped with a Lynx-eye-superspeed detector using Cu K radiation (Bruker, MA, USA).

2.3.5. Microscopy and microanalysis

The gold TEM grids were recovered from the dialysis units by gentle flushing with distilled water onto

a 0.22-μm Millipore filter paper (MA, USA). Washing of the grids was then done under vacuum filtration (moderate pressure) with distilled water, three times. The grids were then allowed to dry prior to imaging. For the final imaging and analysis under high-vacuum SEM, grids representing different reactors were gold (Au) and palladium (Pd) coated using a Model 682 Precision Etching and Coating System (PECS™) by GATAN Inc. (PA, USA). A Quanta™ FEG 250 SEM by FEI (OR, USA) equipped with a field emission gun, secondary, backscattered, and gaseous secondary electron detectors was used to image samples in high vacuum. All micrographs were collected at accelerating voltages between 2 and 5 keV. The elemental microanalysis of specified regions on the microscopy samples was performed by an SEM integrated EDAX Energy Dispersive X-ray Spectroscopy (EDX) system using the TEAM™ software (NJ, USA). In TEAM™ EDX phase mapping, the phase identification occurs simultaneously while the primary map data are collected. It allows efficient microanalysis of samples with meniscal volumes with no prior knowledge of the sample chemistry. A comparison of the composition at each pixel begins from the first frame of the analysis and the quality of the phase definition improves with subsequent frames. The spectra of each phase saved at the end of the analysis can be readily quantified after applying appropriate analysis and corrections for drift and escape peaks (e.g. ZAF corrections). In this study, the EDX data were collected at accelerating voltages between 15 and 20 keV. An effort was made to keep the data collection parameters consistent throughout the examination to facilitate meaningful quantitative comparisons. In addition to areal phase mapping, samples were also subjected to transect microanalysis conducted along a straight line comprising 120 sampling points.

3. Results and discussion

3.1. EPS characterization

Cultures grown for EPS extraction showed the ability to produce copious EPS after 4 days of incubation, at approximately 2.798 mg/mL (Supplementary Table S2). Purified extracts indicated that the EPS composition was largely insoluble in ethanol (76.3% by weight). Presence of carboxylated polysaccharide and sulfated polysaccharide groups was confirmed by the selective retention of Alcian Blue at pH 0.5 and 2.5, respectively (Supplementary Figures S2(a)–(h)). Similar functional groups (carboxylic acid, sulfinic acid, sulfonic acid, and thiols) have been found in the EPS of various *Desulfobacter* spp. in past studies from mildly acidic to mildly alkaline pH [20,34]. Carbohydrate content was determined to be approximately 0.0495 mg/mL in glucose equivalents. Overall, the EPS yield from the 4-day old culture was found to be higher than values reported in previous studies where EPS was extracted from 14-day old *Bacillus* [21] and 21-day old *Dunaliella salina* cultures [35] using similar procedures.

3.2. Solution chemistry and microbial community analysis

Sulfate-reducing activity was achieved in all reactors based on bulk solution sulfate concentrations, with the exception of the control where sulfate concentrations did not diminish over the course of the experiment (results not shown). Note that sulfate concentrations were also found to drop in the EPS-only reactor as well over the incubation period, indicating the possibility of either bioactivity (i.e. survival of SRB, possibly in sporulated form, despite the harsh alcohol washing-based EPS extraction procedure) or the removal of sulfate in the form of a mineral precipitate. The EPS-only reactor also displayed dissolved Ca^{2+} and Mg^{2+} contents to increase across the reactors over two weeks of incubation owing to the administration of increasing Ca^{2+}- and Mg^{2+}-rich replacement media after every sampling event. While the experimental reactors did not exhibit significant differences in the way their Ca^{2+} and Mg^{2+} contents changed over 16 d, measured Ca^{2+} and Mg^{2+} levels at Day 8 and Day 16 were the lowest in Reactor C (EPS-only) (Supplementary Figure S3). Over the course of the experiment, approximately 200 mg of magnesium was estimated to have deposited from the bulk solution data. These results point to a shortcoming of the experimental setup in connecting the Mg recovery in the bulk solution to the recovery in the dialysis tubes and on the TEM grids.

DGGE band profile comparison using bacteria enriched from the sabkha samples (experimental inoculum) against a pure strain of *D. brasiliensis* showed a close similarity in terms of melting behavior (Supplementary Figure S4). The close similarity in melting behavior of a particular band between the enriched SRB community used as the inoculum and *D. brasiliensis* indicated the dolomite-mediating species' presence in the inoculated reactors as well as the original sabkha environment. This result corroborates a previous study by Bontognali et al.[36] where a dolomite-mediating isolate from the Abu Dhabi sabkha to closely match (99.6% identity) *D. brasiliensis* originating from the geographically distant region of Lagoa Vermelha, Brazil [37].

3.3. Mineralogy using XRD

At the scale of this experiment, the total mass of minerals on the grids was considerably small, making XRD analysis exceptionally challenging. Therefore, confirmatory XRD analysis was performed only on minerals associated with the broth of dialysis tubes recovered from Reactors A (bacteria-only) and B (bacteria + EPS). The main peaks of the XRD spectra (Supplementary Figure S5) related to halite and metal oxide–chloride in the dialysis broth. Both minerals were interpreted as artifacts due to the dried growth medium (halite) and to metal oxide–chloride residues from bleach treatment. However, the XRD spectra also included peaks consistent with carbonate minerals with a d104 *p*-value of 3.04 Å, and 3.03 Å. These values corresponded to calcite and Mg–calcite; however, the results cannot be considered a confirmation of abundant carbonate deposition. The XRD spectra did not reveal the presence of phosphate-rich minerals (e.g. apatite and struvite), suggesting that the P peak detected in the later EDX analyses (Figs. 2(e), (f) and Supplementary Figure S6) did not derive from a mineral phase. Rather it may be due to phosphorus associated with the organic molecules within the system [20,34]. XRD attempted on TEM grid samples also resulted in an overwhelming Au peak in the profile spectra restricting applicability of this technique in direct on-grid mineralogical confirmation. Given the limitations with XRD analysis at our experimental scale, supplemental TEM techniques (unavailable during this study) directly applied to the grids would complement the grid-based strategy in future work.

3.4. SEM and EDX on ultrastructures (>50 μm)

Examination of recovered grids revealed rod-shaped bacterial cells measuring 2–3 μm, which were distinguishable in inoculated reactors A and B. While Reactor A presented very few randomly distributed single cells or pairs across the grid surface, Reactor B presented cells occurring in dense aggregates across the substratum. Absence of surface-attached growth in Reactor A suggests that the community could not produce sufficient *de novo* EPS to support bacterial attachment or any mineral nucleation on the substratum over the 16-day incubation period. Prominent insoluble structures measuring greater than 50 μm across (from here onward referred to as "ultrastructures") were distinguishable in Reactors B and C, which were both supplemented with pre-extracted EPS (Figs. 2(a) and (b)). These ultrastructures were generally wider than they were thick, and the one observed in Reactor B appeared to be composed of fused globular units measuring less than 1 μm in diameter. The ultrastructures were most likely large fragments of administered pre-extracted EPS that had attached to the substratum, given that these ultrastructures were absent from Reactor A and the Control reactor grids, and they incorporated mineral components over the incubation period as indicated later by EDX analysis.

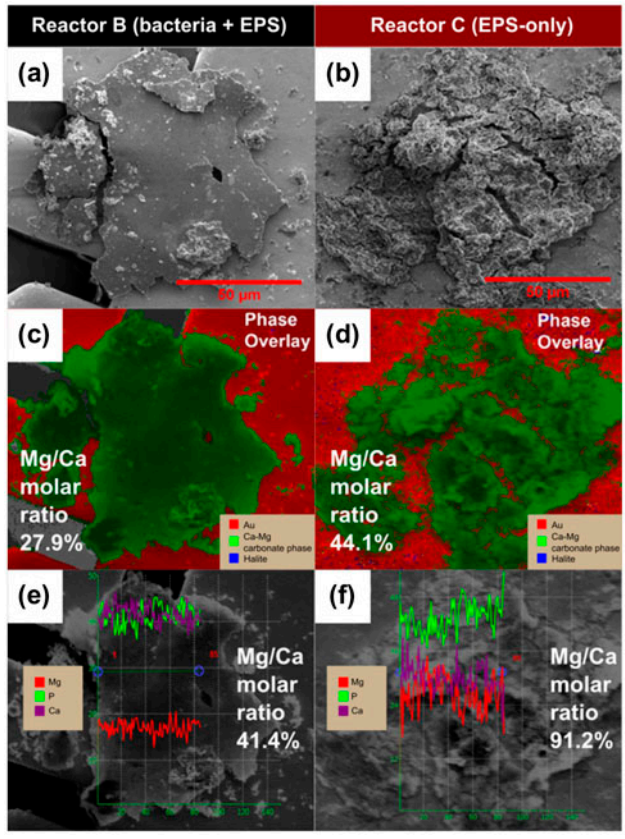

Fig. 2. Comparison of greater surface-attached ultrastructures (>50 m across) found in Reactor B (bacteria + EPS) and Reactor C (EPS-only). (c and d) Phase maps for the two structures of interest, generated from areal analysis of Ca–Mg elemental distribution across these structures. Each color represents a separate phase (green = Ca–Mg, red = Au, blue = NaCl). The elemental distribution in each reactor (by relative atomic percentage) is as follows: Reactor B = 19.95% C, 10.7% Ca, 52.95% O, 2.98% Mg and 13.41% P; and Reactor C = 45.32% C, 4.46% Ca, 41.01% O, 1.97% Mg and 7.24% P. (e and f) Elemental microanalysis was also performed along a line transect across each microstructure, and their Mg/Ca molar ratios calculated. The Mg/Ca molar ratio was observed to be higher in Reactor C, with nearly equal distribution of Mg and Ca across the grid surface. However, it was also noted that values measured using the transect approach were consistently higher than those determined via areal sampling, highlighting a potential bias in investigating elemental distribution with SEM-EDX.

Grid regions from Reactors B and C were screened using EDX for elemental signatures of interest corresponding to Ca–Mg content and the cellular/EPS organic matter content (i.e. C, O, and P [20]). Fig. 2(c) and (d) show a comparison of Ca–Mg phase maps generated over these areas of interest by conducting EDX in low magnification mode (50-μm scale). All regions consistently presented calcium and magnesium alongside the ubiquitous carbon, oxygen, and phosphorus, though at varying levels. The areally averaged EDX spectra of the dominant Ca–Mg phases (green-colored area in Fig. 2(c) and (d)) associated with the selected mineral deposits observed in Reactor B and Reactor C are presented in Supplementary Figure S6. Overall, there was greater incorporation of Mg^{2+} in the ultrastructure found in Reactor C (Mg/Ca molar ratio of 44.1%) than in Reactor B (Mg/Ca ratio of 27.9%). Fig. 2(e) and (f) present the comparison of two sampling transects (a different averaging method) designated across the ultrastructures (Reactor B vs. Reactor C), revealed an even higher Mg/Ca molar ratio (91.2%) in Reactor C than in Reactor B (41.4%). While the absolute numbers of Ca–Mg content obtained via different averaging methods involving EDX analysis might not be reliable in themselves, the comparison between the analysis of grids from the different reactors using a consistent methodology does indicate that ultrastructures in EPS-only systems (Reactor C) produced approximately twice as much Mg incorporation than EPS + bacteria systems (Reactor B). The widespread distribution of Ca^{2+} and Mg^{2+} across the ultrastructures seen in Reactors B and C (Fig. 2(c)–(f)) demonstrates the attraction of Ca^{2+} and Mg^{2+} toward the significant negative charge of the EPS present. In a previous study by Braissant et al.[20], EPS from SRB were observed to present a strong potential to exchange protons and Ca^{2+} ions with the surrounding microenvironment. On the other hand, Bontognali et al.[11] previously reported that EPS from the coastal sabkha microbial mats preferentially bound Mg^{2+} and Si^{4+} in the early stages of mineralization.

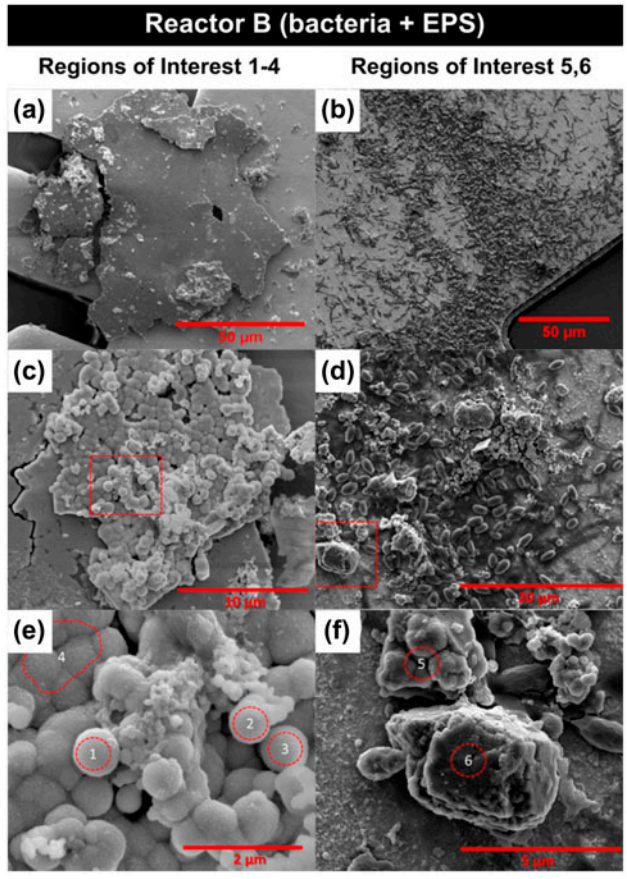

Fig. 3. ROIs in Reactor B revealing divergent morphologies; with (a), (c), and (e) representing sites with thick cover, and (b), (d), and (f) representing areas of high cell density and visible granulations. Numbered sections indicate sites examined with elemental microanalysis to determine their compositions. The calculated Mg/Ca molar ratios are as follows: ROIs 1–3, averaged = 23%; ROI 4 = 19.9%; ROI 5 = 27.2%; and ROI 6 = 61.9%. ROIs 5 and 6 presented distinct inorganic formations against the landscape of rod-shaped cells and extracellular secretions on the substratum. The observed deposits most likely arose from nucleating sites across the substratum, budding into larger crystals (ROI 5) that might coalesce with neighboring formations within microscopic distances from each other (ROI 6). Peak profiles for these ROIs are presented by Supplementary Figures S7 and S8.

3.5. Detailed SEM and EDX on microstructures (<10 μm) in EPS+bacteria reactor

Unlike Reactor C (EPS-only), Reactor B (bacteria + EPS) presented a variety of mineral deposition morphologies in association with culture growth beyond the prominent ultrastructures (Fig. 3(a)). Trails with a distinct contrast were found widely across various regions of the grid, particularly in association with cells (Fig. 3(b) and (d)) with some trails appearing to be exuded by individual cells, indicating *de novo* EPS generation to support surface-attached growth. Peak cell attachment per normalized grid area, estimated from the SEM micrographs (Supplementary Information), was found to be approximately 18 cells/100 μm^2 in Reactor B (bacteria + EPS) when compared to only 4 cells/100 μm^2 for Reactor A (bacteria-only control reactor). Granular deposits of varying sizes and thicknesses were also observed among the cells and extracellular materials (Fig. 3(d) and (f)). These deposits

appeared largely inorganic judging by their granular morphology. These granular microstructures could possibly be mineral precipitates in various stages of growth—although this inference cannot be concluded because SEM-–EDX analysis, a destructive technique, was performed only at the end of the 16-day experiment. The smallest units observed appeared as clusters of submicron spheres (Fig. 3(f), Region of Interest (ROI) 5) with distinct contrast on otherwise flat amorphous surfaces; while advanced structures up to 5 μm long (Fig. 3(f), ROI 6) could be seen in close association with large cell populations.

In the interest of evaluating their composition, these ROIs in Reactor B were compared using spot EDX analysis. Regions with more amorphous features (ROIs 1–4, Fig. 3(c) and (e)) exhibited a relatively low Mg/Ca molar ratio (approximately 21.4%) compared to regions presenting more granular structures (ROIs 5 and 6, Fig. 3(f)) with a Mg/Ca molar ratio of up to 61.9% (ROI 6). The detailed examination of the ROIs in Reactor B pointed to a significant incorporation of Mg^{2+} into the more granular surface deposits. This might support the hypothesis speculated by some of gradual Mg incorporation into calcite or aragonite [38–40].

A shift in phosphorus content across the ROIs was also noted, with the highest quantity observed in the section of ultrastructure examined (ROIs 1 through 4) and none detected in the distinct structure of ROI 6 (data not shown). In addition to the high Mg/Ca ratio in the ROI 6 formation, the absence of phosphorus could be another indicator of the precipitated mineral's late stage of growth. The absence of phosphate mineral peaks in the earlier confirmatory XRD analysis of Reactor B samples also ruled out the possibility of artifacts such as apatite and struvite depositing out of the growth media [41]. These data suggest a trend of mineral deposition away from an actively growing/unsaturated EPS framework. EPS, the chief component of the biofilm matrix, can act as a phosphorus reservoir in the studied microbial communities, owing to the EPS' ability to accumulate phosphorus from the surroundings, and the possible presence of phosphate-rich molecules in the matrix [42,43].

3.6. Relevance to targeted Mg recovery from brines

The advantage of a potential process for magnesium recovery from brines that is based on biomineralization lies in its selectivity for magnesium sequestration, as well as its low-energy demand over existing processes (e.g. Pidgeon and Dow processes) because of operation under ambient conditions. Still, before such a process can be commercially viable, a clear understanding of the fundamental science behind the process is necessary. Another bottleneck to the commercial viability of this process is its requirement of biologically generated EPS, which requires biological culture growth and EPS extraction. With a better understanding of the role of EPS in the process, prevalent synthetic chemical surrogates could potentially be utilized instead. On this note, there has been some success in the employment of polyanionic surrogates of EPS for carbonate deposition. For example, recent abiotic experiments demonstrated an instrumental role of polysaccharides like carboxymethyl cellulose and agar in conditioning the surfaces of nucleating calcite "seed" crystals within simulated sulfate-free and increasingly alkaline environments [23]. Note that sulfate-reducing conditions might still be necessary, especially for a greater extent of magnesium recovery in the form of Ca–Mg carbonates, because of their role in breaking up the magnesium and sulfate ion pairing [44].

4. Conclusions

A novel methodology was employed to demonstrate the precipitation of Ca–Mg recovery only in pre-extracted EPS-bearing Reactors B and C, indicating that pre-extracted EPS was necessary for magnesium sequestration under sulfate-reducing conditions. The absence of deposits in Reactors A (bacteria-only) and the control indicated that Ca–Mg minerals were not a product of spontaneous precipitation from sterile, increasingly hypersaline media, and that microbial cells alone were insufficient to drive deposition. Overall, magnesium incorporation into the EPS-only system was uniformly $1.5x-2.2x$ greater compared to the bacteria + EPS system when comparing large surface deposition "ultrastructures." However, analysis of microstructures within Reactor B (bacteria + pre-extracted EPS) system revealed variations in the Mg/Ca molar ratios ranging from 19.9 to 61.9% with a concomitant decrease in phosphorus content over different morphologies, indicating a possible dynamic mineralization process that will require further investigation. The study represents an initial proof-of-concept of a promising potentially low-energy beneficial mineral recovery process utilizing aqueous saline waste streams such as desalination brine. Further investigations are needed to understand the mechanism of magnesium recovery from seawater brines.

Supplementary material

The supplementary material for this paper is available online at http://dx.doi.[10.1080/19443994.2016.1155179].

Acknowledgments

The authors would like to thank the Masdar Institute of Science and Technology for funding this research.

References

[1] W. Wulandari, G.A. Brooks, M.A. Rhamdhani, B.J. Monaghan, Magnesium: Current and alternative production routes, Chemeca, Engineering at the Edge; 26–29 September 2010, Hilton Adelaide, South Australia (2010) 347.
[2] G. Brooks, M. Cooksey, G. Wellwood, C. Goodes, Challenges in light metals production, Miner. Process. Extr. Metall. 116 (2007) 25–33.
[3] D.A. Kramer, Magnesium, Its Alloys and Compounds, US Department of the Interior, US Geological Survey, 2001.
[4] I. Al Mutaz, K. Wagialia, Production of magnesium from desalination brines, Resour. Conserv. Recycl. 3 (1990) 231–239.
[5] A. Ravizky, N. Nadav, Salt production by the evaporation of SWRO brine in Eilat: A success story, Desalination 205 (2007) 374–379.
[6] D.H. Kim, A review of desalting process techniques and economic analysis of the recovery of salts from retentates, Desalination 270 (2011) 1–8.
[7] S. Adham, A. Hussain, J.M. Matar, R. Dores, A. Janson, Application of membrane distillation for desalting brines from thermal desalination plants, Desalination 314 (2013) 101–108.
[8] M.C. Brook, H. Al-Houqani, T. Darawsha, M. Al-Alawneh, S. Achary, Groundwater Resources: Development and management in the Emirate of Abu Dhabi, United Arab Emirates, in: A.M.O. Mohamed (Ed.), Arid Land Hydrogeology, In Search of a Solution for a Threatened Resource Taylor & Francis, London, 2006, pp. 14–34.
[9] Dornier Consulting, Hydrogeology Study for the Masdar Development, 2009.
[10] J.L. Imes, W.W. Wood, Solute and isotope constraint of groundwater recharge simulation in an arid environment, Abu Dhabi Emirate, United Arab Emirates, Hydrogeol. J. 15 (2007) 1307–1315.
[11] T.R.R. Bontognali, C. Vasconcelos, R.J. Warthmann, S.M. Bernasconi, C. Dupraz, C.J. Strohmenger, J.A. Mckenzie, Dolomite formation within microbial mats in the coastal sabkha of Abu Dhabi (United Arab Emirates), Sedimentology 57 (2010) 824–844.
[12] S. Deng, H. Dong, G. Lv, H. Jiang, B. Yu, M.E. Bishop, Microbial dolomite precipitation using sulfate reducing and halophilic bacteria: Results from Qinghai Lake, Tibetan Plateau, NW China, Chem. Geol. 278 2010 151–159.
[13] M. Sánchez-Román, C. Vasconcelos, R. Warthmann, M. Rivadeneyra, J.A. McKenzie, Microbial dolomite precipitation under aerobic conditions: Results from Brejo do Espinho Lagoon (Brazil) and culture experiments, Perspectives in Carbonate Geology A Tribute to the Career of Robert Nathan Ginsburg, Wiley-Blackwell, UK, 2009, pp. 167–178.
[14] M. Sanz-Montero, J. Rodríguez-Aranda, Magnesite formation by microbial activity: Evidence from a Miocene hypersaline lake, Sediment. Geol. 263–264 (2012) 6–15.
[15] C. Vasconcelos, R. Warthmann, J.A. McKenzie, P.T. Visscher, A.G. Bittermann, Y. van Lith, Lithifying microbial mats in Lagoa Vermelha, Brazil: Modern Precambrian relics? Sediment. Geol. 185 (2006) 175–183.
[16] C. Vasconcelos, J.A. McKenzie, Dolomite as a biomineral and possible implications, Macla 49 (2008) 21–25.
[17] R. Warthmann, Y. van Lith, C. Vasconcelos, J.A. McKenzie, A.M. Karpoff, Bacterially induced dolomite precipitation in anoxic culture experiments, Geology 28 (2000) 1091.
[18] H.-C. Flemming, J. Wingender, The biofilm matrix, Nat. Rev. Microbiol. 8 (2010) 623–633.
[19] S. Tsuneda, H. Aikawa, H. Hayashi, A. Yuasa, A. Hirata, Extracellular polymeric substances responsible for bacterial adhesion onto solid surface, FEMS Microbiol. Lett. 223 (2003) 287–292.
[20] O. Braissant, A.W. Decho, C. Dupraz, C. Glunk, K.M. Przekop, P.T. Visscher, Exopolymeric substances of sulfate-reducing bacteria: Interactions with calcium at alkaline pH and implication for formation of carbonate minerals, Geobiology 5 (2007) 401–411.
[21] C. Ercole, P. Cacchio, A.L. Botta, V. Centi, A. Lepidi, Bacterially induced mineralization of calcium carbonate: The role of exopolysaccharides and capsular polysaccharides, Microsc. Microanal. 13 (2007) 42–50.
[22] M. Sánchez-Román, J.A. McKenzie, A. de Luca Rebello Wagener, M.A. Rivadeneyra, C. Vasconcelos, Presence of sulfate does not inhibit low-temperature dolomite precipitation, Earth Planet. Sci. Lett. 285 (2009) 131–139.
[23] F. Zhang, H. Xu, H. Konishi, E.S. Shelobolina, E.E. Roden, Polysaccharide-catalyzed nucleation and growth of disordered dolomite: A potential precursor of sedimentary dolomite, Am. Mineral. 97 (2012) 556–567.
[24] J.R. Postgate, The sulphate-reducing bacteria, CUP Archive, 1979, pp. 24–40.
[25] C.-C. Hung, P.H. Santschi, J.B. Gillow, Isolation and characterization of extracellular polysaccharides produced by *Pseudomonas fluorescens* Biovar II, Carbohydr. Polym. 61 (2005) 141–147.
[26] B.C. Richter, C.W. Kreitler, Geochemical Techniques for Identifying Sources of Ground-water Salinization, CRC, Boca Raton, FL, 1993.
[27] C.M. Bethke, Geochemical and Biogeochemical Reaction Modeling, Cambridge University Press, 2007.
[28] C.E. Harvie, N. Møller, J. Weare, The prediction of mineral solubilities in natural waters: The Na-K-Mg-Ca-H-Cl-SO_4-0H-HCO_3-CO_3-CO_2-H_2O system to high ionic strengths at 25°C, Geochim. Cosmochim. Acta 48 (1984) 723–751.
[29] C.A. Appel, T.E. Reilly, Summary of Selected Computer Programs Produced by the US Geological Survey for Simulation of Ground-water Flow and Quality, 1994, USGPO, 1994.
[30] Y. Tamaru, Y. Takani, T. Yoshida, T. Sakamoto, Crucial role of extracellular polysaccharides in desiccation and freezing tolerance in the terrestrial

cyanobacterium *Nostoc commune*, Appl. Environ. Microbiol. 71 (2005) 7327–7333.
[31] M. DuBois, K.A. Gilles, J.K. Hamilton, P. Rebers, F. Smith, Colorimetric method for determination of sugars and related substances, Anal. Chem. 28 (1956) 350–356.
[32] A. Farhat, A.N. Dooley, F. Ahmad, Nitrite oxidation in ion chromatography-electrospray ionization-tandem mass spectrometry (IC-ESI-MS/MS), J. Mass Spect. 46 (2011) 720–724.
[33] M. Mieseler, M.N. Atiyeh, H.H. Hernandez, F. Ahmad, Direct enrichment of perchlorate-reducing microbial community for efficient electroactive perchlorate reduction in biocathodes, J. Ind. Microbiol. Biotechnol. 40 (2013) 1321–1327.
[34] O. Braissant, A.W. Decho, K.M. Przekop, K.L. Gallagher, C. Glunk, C. Dupraz, P.T. Visscher, Characteristics and turnover of exopolymeric substances in a hypersaline microbial mat, FEMS Microbiol. Ecol. 67 (2009) 293–307.
[35] A. Mishra, B. Jha, Isolation and characterization of extracellular polymeric substances from micro-algae *Dunaliella salina* under salt stress, Bioresour. Technol. 100 (2009) 3382–3386.
[36] T.R. Bontognali, C. Vasconcelos, R.J. Warthmann, R. Lundberg, J.A. McKenzie, Dolomite-mediating bacterium isolated from the sabkha of Abu Dhabi (UAE), Terra Nova 24 (2012) 248–254.
[37] R. Warthmann, C. Vasconcelos, H. Sass, J.A. McKenzie, *Desulfovibrio brasiliensis sp. nov.*, a moderate halophilic sulfate-reducing bacterium from Lagoa Vermelha (Brazil) mediating dolomite formation, Extremophiles 9 (2005) 255–261.
[38] P.A. Baker, M. Kastner, Constraints on the formation of sedimentary dolomite, Science 213 (1981) 214–216.
[39] J.S. Compton, Degree of supersaturation and precipitation of organogenic dolomite, Geology 16 (1988) 318–321.
[40] S. Mazzullo, Organogenic dolomitization in peritidal to deep-sea sediments, J. Sediment. Res. 70 (2000) 10.
[41] K.L. Gallagher, O. Braissant, T.J. Kading, C. Dupraz, P.T. Visscher, Phosphate-related artifacts in carbonate mineralization experiments, J. Sediment. Res. 83 (2013) 37–49.
[42] Z. Zhang, X. Huang, H. Yang, K. Xiao, X. Luo, H. Sha, Y. Chen, Study on P forms in extracellular polymeric substances in enhanced biological phosphorus removal sludge by ^{31}P-NMR spectroscopy, Spectrosc. Spec. Anal., 29 (2009) 536.
[43] T.E. Cloete, D.J. Oosthuizen, The role of extracellular exopolymers in the removal of phosphorus from activated sludge, Water Res. 35 (2001) 3595–3598.
[44] L.S. Land, Failure to precipitate dolomite at 25° C from dilute solution despite 1000-fold oversaturation after32 years, Aquat. Geochem. 4 (1998) 361–368.